frontiers | Frontiers in Marine Science

TYPE Original Research
PUBLISHED 03 December 2024
DOI 10.3389/fmars.2024.1500949

OPEN ACCESS

EDITED BY
Juan Jose Munoz-Perez,
University of Cádiz, Spain

REVIEWED BY
Li Wu,
Anhui Normal University, China
Zhongbo Wang,
Shantou University, China

*CORRESPONDENCE
Xiaomei Nian
xmnian@sklec.ecnu.edu.cn

RECEIVED 24 September 2024
ACCEPTED 14 November 2024
PUBLISHED 03 December 2024

CITATION
Nian X, Zhang W, Wang X and Qiu F (2024) Holocene evolution of the buried tidal sand body in the North Jiangsu Plain of China revealed by luminescence dating. *Front. Mar. Sci.* 11:1500949. doi: 10.3389/fmars.2024.1500949

Holocene evolution of the buried tidal sand body in the North Jiangsu Plain of China revealed by luminescence dating

Xiaomei Nian*, Weiguo Zhang, Xuemei Wang and Fengyue Qiu

State Key Laboratory of Estuarine and Coastal Research, East China Normal University, Shanghai, China

In the northern Jiangsu coastal zone of China, the buried tidal sand body (BTSB) is suggested to share a similar origin with the offshore radial sand ridge system in the southwestern Yellow Sea. However, its chronological framework remains inadequately understood. This study conducted optically stimulated luminescence (OSL) dating of both silt- and sand-sized quartz on core LDC from the southwestern end of the BTSB. Together with data from the previously studied core XYK closer to the current coastline, this study aims to clarify the chronology of the BTSB and refine its evolution history. The results indicate that in both cores, sand-sized quartz provides more reliable age estimates than silt-sized quartz for the sandy sediment layers. Additionally, the discrepancy between ages derived from the single-grain central age model and the minimum age model is smaller within the top 11 m of the core, which was deposited over the last 0.9 ka. This period corresponds well with the southern migration of the Yellow River and its sediment discharge into the Yellow Sea from 1128 to 1855 CE. It suggests that distinct sediment sources from the Yellow and Yangtze Rivers may account for the observed differences in OSL characteristics. The OSL ages reveal significant temporal variations in sedimentation rates during the Holocene, with the most rapid deposition occurring between 1.2–0.4 ka and 10–8 ka in core LDC, and between 2–1 ka in core XYK. Together with dating results from the central part of the BTSB, it reveals complex spatiotemporal variations in sediment accumulation and emphasizes the need for detailed sediment sampling and dating to fully elucidate the evolutionary history of the coastal plain.

KEYWORDS

tidal sand body, optically stimulated luminescence (OSL) dating, Holocene evolution, single grain, sediment source

1 Introduction

Tidal sand ridges are commonly found in continental shelf and coastal regions where there are abundant sands and the presence of tidal currents (Dyer and Huntley, 1999). The radial tidal sand ridge system in the southwestern Yellow Sea, spanning over 20,000 km² of the continental shelf (Figure 1), is one of the world's most spectacular landscapes (Wang, 1982). This fan-shaped system, extending seaward from Jianggang, has been widely studied regarding its evolutionary process and sediment source, offering valuable insights into the geomorphology of the coastal sea in eastern China (Yang, 1985; Li and Zhao, 1995; Li et al., 2001; Wang, 2014).

Adjacent to this offshore radial tidal sand ridge system, a semi-circular area spanning about 3,000 km² on the North Jiangsu coastal plain features dominant sandy deposits in the Holocene sedimentary sequence (Li et al., 2001). The sandy deposits are suggested to have a common tidal origin with the offshore sand ridges, and thus referred to as the buried tidal sand body (BTSB) (Li et al., 1999). Previous studies have suggested that the BTSB was formed around 6–5 ka BP (Li et al., 1999), which is younger than the tidal sand ridges formed in the paleo-incised valley of the Yangtze River (11.5–7 ka BP) (Liu et al., 2020), but older than the radial sand ridge system on the Yellow Sea shelf (Li et al., 2001). However, dating results are scarce from the BTSB area (e.g., Li et al., 2001; He et al., 2023), and therefore the chronological framework of the BTSB remains unclear. Part of the reason is the absence of carbon-containing material in the sandy deposit for the conventional ^{14}C dating method.

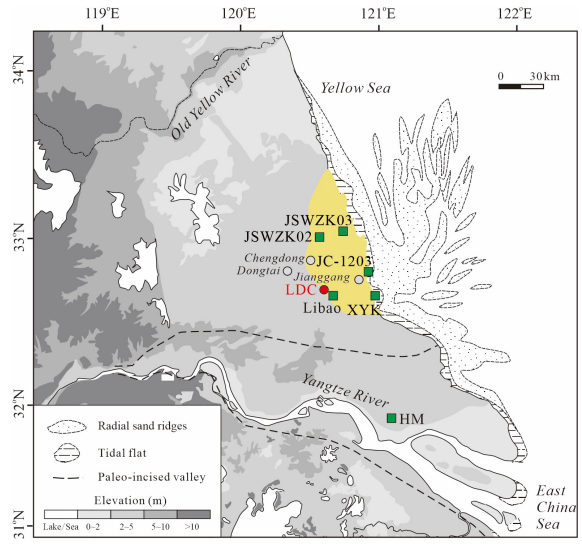

FIGURE 1
Tidal sand ridge system in the northern Jiangsu Plain and southern Yellow Sea (modified from Li et al., 2001). The yellow shaded area represents the buried tidal sand body (BTSB), while the white dotted area indicates the offshore tidal sand ridge. The dashed line delineates the boundary of the paleo-incised Yangtze valley formed in the late Pleistocene (Li et al., 2000). The red circle marks the location of core LDC. Green squares denote the locations of cores from previous studies, including cores Libao (Chen et al., 1994), JC-1203 (Xiao, 2015), HM (Nian et al., 2021), XYK (Nian et al., 2022a), JSWZK02 and JSWZK03 (He et al., 2023).

Optically stimulated luminescence (OSL) dating has become a valuable tool for establishing the ages of sandy deposits in coastal settings, particularly where organic material is scarce (e.g., Jacobs, 2008; Nian and Zhang, 2018; Gao et al., 2022; Liu et al., 2022; Nian et al., 2022a, 2022b; Xu et al., 2022; Lin et al., 2023). However, in coastal environments with changing hydrodynamics and rapid erosion-deposition cycles, OSL dating can be affected by age discrepancies between different grain sizes (Cheng et al., 2020; Nian et al., 2021; Niu et al., 2022). In our previous study on a core from the BTSB, we found that sand-sized quartz OSL results are more reliable than those of silt-sized grains, which was interpreted to be the result of lateral erosion of sand ridges and the infiltration of younger fine-grained sediments into the sandy body (Nian et al., 2022a). This underscores the need to understand sedimentation dynamics and carefully select appropriate grain sizes to accurately reconstruct depositional history.

This study aims to refine the chronological framework of the BTSB by conducting OSL dating on a new core from the southwestern part of the BTSB. By integrating the OSL results with existing studies, we seek to enhance our understanding of the BTSB's evolutionary history. The findings from this research are expected to provide insights into the study of tidal sand ridge formation in coastal environments elsewhere.

2 Samples and methods

The BTSB region is situated between the Yangtze River Delta to the south and the abandoned Yellow River Delta to the north (Figure 1). The sedimentary sequence in the BTSB region consists of a basal paleosol of late Pleistocene, which is overlain by tidal flat/estuary deposits, tidal sand ridge facies, and tidal flat deposits in ascending order (Chen et al., 1994; Li et al., 2001). A ~26 m sediment core LDC (32°36′27.47″N, 120°37′57.78″E, 3.61 m asl) with ~93% recovery was obtained from Lindongcun in the southwest part of the BTSB (Figure 1). The core was divided into two sections: one processed under subdued red light in the luminescence laboratory to prevent sunlight exposure during OSL sample collection, and the other analyzed under natural light for lithological and additional analyses. Based on lithological descriptions, grain-size analysis, and stratigraphic correlation with previously studied core (Chen et al., 1994), the core was stratigraphically divided into four units (Figure 2): U4 (26–25.6 m) consists of gray stiff clay, representing the late Pleistocene paleosol; U3 (25.6–21.8 m) corresponds to tidal flat/estuarine facies characterized by interbedded silts and sands with shell fragments; U2 (21.8–2.7 m) represents a tidal sand ridge facies, consisting of grayish-black silty sands and sands with sporadic shell fragments; and U1 (2.7–0 m) corresponds to tidal flat facies composed of yellow-brown clayey silts.

Grain-size distribution was analyzed using a Beckman Coulter LS 13320 laser particle analyzer, which revealed a dominance of coarse silts and sand fractions (Figure 2; Supplementary Figure S1). Based on these findings, silt-sized (45–63 μm) and sand-sized (90–125 μm) quartz fractions of 17 samples were selected for OSL dating. The OSL samples underwent standard chemical pretreatment, including etching with hydrochloric acid (HCl) and hydrogen peroxide (H_2O_2) to remove carbonates and organic matter, followed by thorough rinsing with

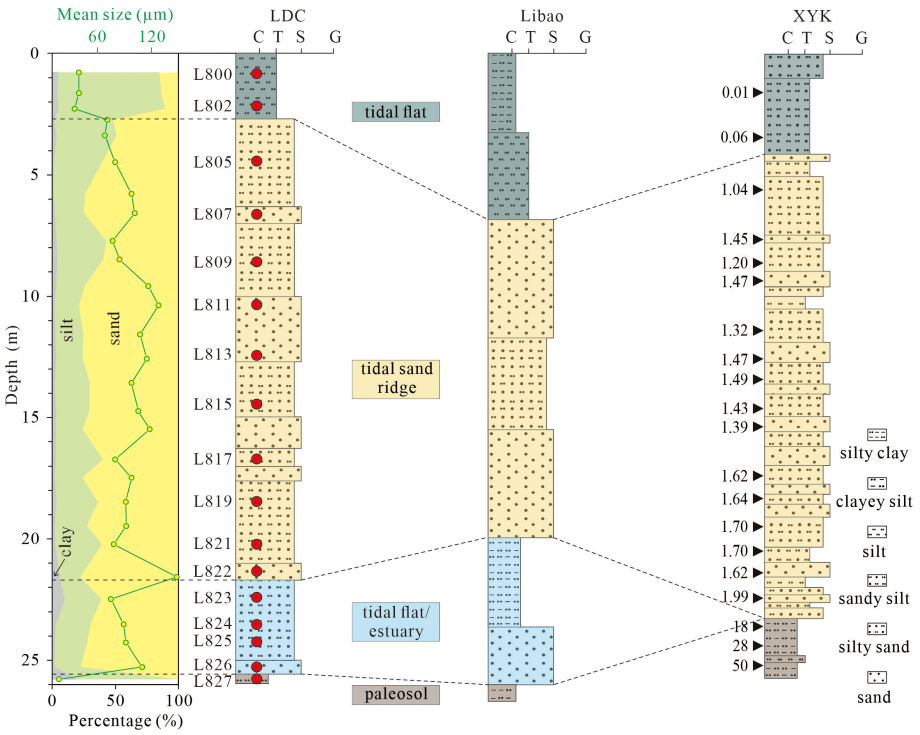

FIGURE 2
Lithological profile of core LDC showing down-core variations in grain size composition and OSL sample locations (red closed circles), along with stratigraphic correlations with nearby cores Libao (Chen et al., 1994) and XYK (Nian et al., 2022a). The triangle in core XYK denotes the OSL age in ka.

distilled water. The samples were then wet-sieved to separate the grains and dried at temperatures below 40°C. To extract pure quartz, the 45–63 μm grains were treated with fluosilicic acid (H_2SiF_6) for 3–5 days, while the 90–125 μm grains were etched with hydrofluoric acid (HF) for 40 mins. A final rinse with HCl and distilled water ensured the removal of residual fluorides. The purity of quartz was verified using infrared stimulation.

The OSL measurements were performed using an automated Risø TL/OSL-DA-20 reader, equipped with an automated detection and stimulation head (DASH) and a beta radiation source ($^{90}Sr/^{90}Y$). The system utilized blue LED stimulation at 470 nm (72 mW cm^{-2}), IR stimulation at 870 nm (130.5 mW cm^{-2}) and green laser stimulation at 532 nm (90 mW cm^{-2}). Detection was conducted with a photomultiplier tube (ET PDM-9107-CP-TTL) with a Hoya U-340 optical filter. A constant heating rate of 5°C s^{-1} was applied during all measurements. The grains were mounted on 9.7-mm-diameter stainless steel discs as small aliquots (2 mm diameter) for single-aliquot OSL dating, while single-grain measurements were carried out on discs with 100 holes, each 300 μm in diameter and depth.

Equivalent dose (D_e) values for single-aliquot and single-grain measurements were estimated following protocols detailed in Supplementary Tables S1 and S2. For single-aliquot measurements, D_e values were calculated by integrating the initial 0.4 s of stimulation. Background correction was performed by subtracting both early (0.4–1.4 s) (Ballarini et al., 2007; Cunningham and Wallinga, 2010) and late (last 10 s) signals. The results from these two background subtraction methods were consistent within experimental error, and the data based on late background subtraction were used in this study. For single-grain measurements, the OSL signal was integrated over the first 0.05 s, with background signals assessed from the final 0.3 s. The D_e values were estimated using both the central age model (CAM) and minimum age model (MAM) (Galbraith et al., 1999). For MAM age calculations, a sigma b (σ_b) value of 10% was applied for the 45–63 μm data and 20% for the 90–125 μm data, consistent with a previous study in the area (Nian et al., 2022a). The age models were selected following Arnold et al. (2007) for single-aliquot measurements, and Bailey and Arnold (2006) for single-grain measurements.

The contents of uranium (U), thorium (Th), and potassium (K) were determined using ICP-MS analysis (Supplementary Table S3). Corrections for cosmic-ray dose rates, alpha and beta attenuation, and alpha efficiency were applied using the same parameters described by Nian et al. (2022a) for core XYK in the study area. Laboratory-measured water content was factored into the dose rate calculations with an uncertainty of ±5%.

3 Results

3.1 The single-aliquot data for 45–63 μm quartz

Figure 3A presents a representative natural OSL decay curve and the associated dose-response curve for 45–63 μm quartz grains, obtained using the single-aliquot regenerative-dose (SAR) protocol (Supplementary Table S1). The stimulation curve indicates that the OSL signals are dominated by the fast component, consistent with the

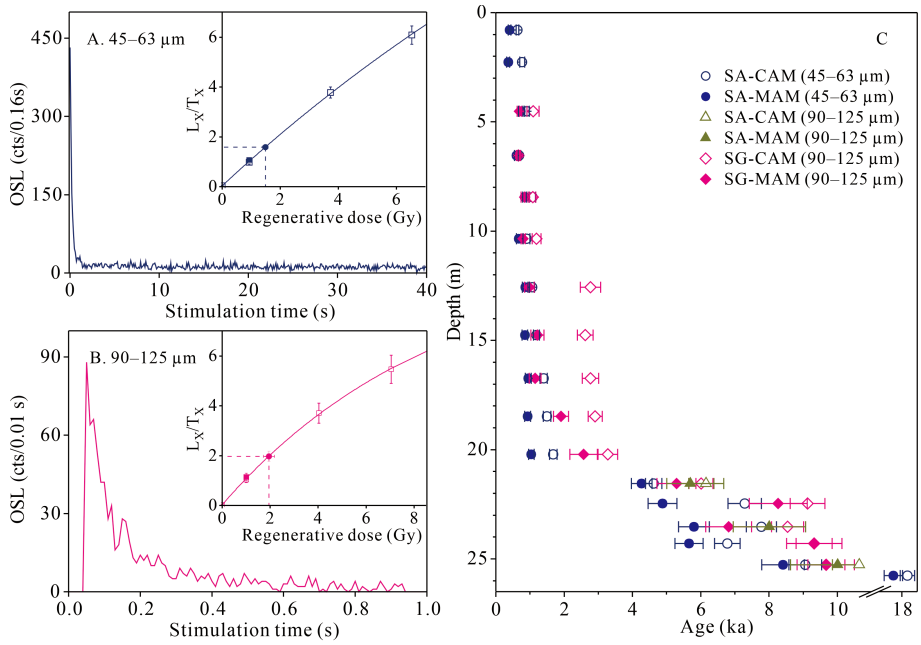

FIGURE 3
The natural OSL decay curves and their corresponding sensitivity-corrected growth curves for **(A)** 45–63 μm single-aliquot (SA) and **(B)** 90–125 μm single-grain (SG) quartz in sample L807. **(C)** The OSL dating results obtained using different grain sizes and protocols. Open blue circles, dark-yellow triangles, and pink rhombuses represent the CAM ages for 45–63 μm SA, 90–125 μm SA, and 90–125 μm SG quartz, respectively, while the corresponding closed symbols represent their MAM ages. The detailed dating results are presented in Supplementary Tables S5, S6, and S8.

luminescence characteristics of quartz observed in the Yangtze River Delta (Nian et al., 2019) and core XYK (Nian et al., 2022a) in the study area. To assess the robustness and reliability of the SAR protocol employed, dose recovery tests were performed based on the approach outlined by Wintle and Murray (2006). In these tests, natural OSL signals were subjected to a two-step bleaching process using blue LED stimulation, each lasting 40 s and separated by a pause exceeding 10,000 s at room temperature. After bleaching, the aliquots were given a known laboratory dose and subsequently measured using the SAR protocol detailed in Supplementary Table S1. The dose recovery ratios for the nine samples analyzed ranged from 0.9 to 1.1 (Supplementary Table S4), confirming the accuracy and validity of the SAR protocol for these samples.

The overdispersion (OD) values of quartz D_e from the Holocene sandy layer ranged between 16% and 52% (Supplementary Table S5). Considering that each 2 mm diameter aliquot for the 45–63 μm grain-size fraction comprises ~890 grains (Burow, 2020), such high OD values suggest two main factors: heterogeneous bleaching and low luminescence sensitivity of quartz grains. Figure 3C presents a comparison between the ages derived from the CAM and MAM, showing that CAM ages (0.63–9.06 ka) are generally older than the corresponding MAM ages (0.4–8.41 ka) (Supplementary Table S5).

3.2 The 90–125 μm quartz OSL data

3.2.1 The single-aliquot data for 90–125 μm quartz

Three 90–125 μm quartz samples were also dated using the SAR protocol (Supplementary Table S1). For calculating the MAM D_e values, a σ_b value of 20% was chosen. This selection is consistent with the standard value for single-grain measurements and reflects the low concentration of valid bright grains in these samples (Section 3.2.2) as well as findings from previous studies in the Yangtze River Delta (Nian et al., 2018b, 2019, 2021). The dating results are shown in Supplementary Table S6. The OD values of 90–125 μm D_e distribution ranged from 23% to 48%, which are higher than those observed for the 45–63 μm grain size fraction (15–24%). The CAM ages of the sand-sized samples were 6.16 ± 0.51 ka, 11.41 ± 1.15 ka, and 10.64 ± 0.78 ka, while the corresponding MAM ages were 5.70 ± 0.69 ka, 8.01 ± 1.06 ka, and 10.01 ± 1.38 ka for samples L822, L824, and L826, respectively. Notably, even the MAM values for the sand-sized quartz grains are higher than the corresponding CAM values for the silt-sized grains (Figure 3C).

3.2.2 The single-grain data for 90–125 μm quartz

The single-grain dose recovery experiments for two representative samples followed the same steps as for single aliquots described in Section 3.1. The recovered ratios were 0.98 ± 0.06 and 1.10 ± 0.06 (Supplementary Table S4). Typical dose-response and decay curves are shown in Figure 3B. The standard rejection criteria for single-grain quartz measurements are listed in Supplementary Table S7, with only 0.68% to 3.46% (average 1.36%) of grains meeting these criteria. This low percentage indicates that 'pseudo' single-grain effects (multiple grains per hole) are negligible for these samples. The OD values of D_e distributions for 90–125 μm quartz grains ranged from 17% to 64%, with CAM ages generally slightly higher or comparable to MAM ages, spanning from ~0.66 ka to 9.68 ka (Supplementary Table S8).

4 Discussion

4.1 A robust chronological framework of core LDC

Except for the samples in the upper 11 m of core LDC, the single-grain OSL ages of 90–125 μm quartz (Supplementary Table S8) are consistently older than the single-aliquot ages of 45–63 μm quartz (Supplementary Table S5) (Figure 3C). Abanico plots of D_e distributions indicate that the silt-sized SAR ages are more scattered than the sand-sized OSL ages, exhibiting broader distributions with minor peaks that influence the final age estimates (Figure 4). Previous studies in the Yangtze River Delta have shown that medium component dominance can lead to underestimated single-aliquot OSL ages; however, the single-grain method effectively addresses this issue ages (Nian et al., 2024). Therefore, the consistency between the single-aliquot and single-grain ages of 90–125 μm quartz (Supplementary Tables S6, S8; Figure 3C) in this study suggests that the age differences are not attributable to quartz signal components or measurement protocols.

A similar phenomenon is observed in core XYK in the eastern area, where the 90–125 μm quartz OSL ages are systematically older than the 45–63 μm ages, a discrepancy not attributable to partial bleaching as it contradicts the expected results (Nian et al., 2022a). This age discrepancy is likely influenced by the depositional dynamics of tidal sand ridges, where lateral erosion exposes older deposits, allowing younger, fine-grained sediments to infiltrate through tidal currents (Nian et al., 2022a). This study reinforces previous findings, suggesting that OSL ages derived from fine grains may underestimate the true depositional ages of sandy sediments in highly dynamic environments. Thus, OSL ages from sand-sized grains are considered more reliable for dating tidal sand ridges, as they are less susceptible to post-depositional reworking. To construct the age-depth model for core LDC, we combined the 45–63 μm single-aliquot quartz OSL ages from the top most two samples of tidal flat facies and the bottom sample from the paleosol with the single-grain OSL ages of 90–125 μm quartz for the remaining samples, revealing a general increase in age with depth (Figure 5).

The basal paleosol in core LDC is dated to ~18.7 ka, reflecting its formation during the late Pleistocene (Li et al., 1999) (Figure 2). A sedimentary hiatus separates this paleosol from the overlying Holocene sediments. Clearly, there are significant variations in the sedimentation rate during the Holocene (Figure 2). Sedimentation rates were relatively high (~2 m/ka) during the early Holocene (10–8 ka), but slowed to 0.5–1 m/ka between 8 and 1.2 ka, with a brief increase to ~5 m/ka around 3 ka. From 1.2 to 0.4 ka, sedimentation rates increased dramatically to ~18 m/ka.

4.2 Implications for sediment source change using OSL signals

The differences in single-grain OSL ages from two age models of the same sample display a distinct shift around the 11 m depth in core LDC (Figure 3C). Below this depth, CAM ages derived from sand-sized grains are consistently older than MAM ages, while above this depth, the discrepancies between these two age models become less pronounced. This variation could be explained by incomplete bleaching in the lower section, likely due to deeper water conditions that limited sunlight exposure, thereby hindering the resetting of OSL signals (Wallinga, 2002; Niu et al., 2022).

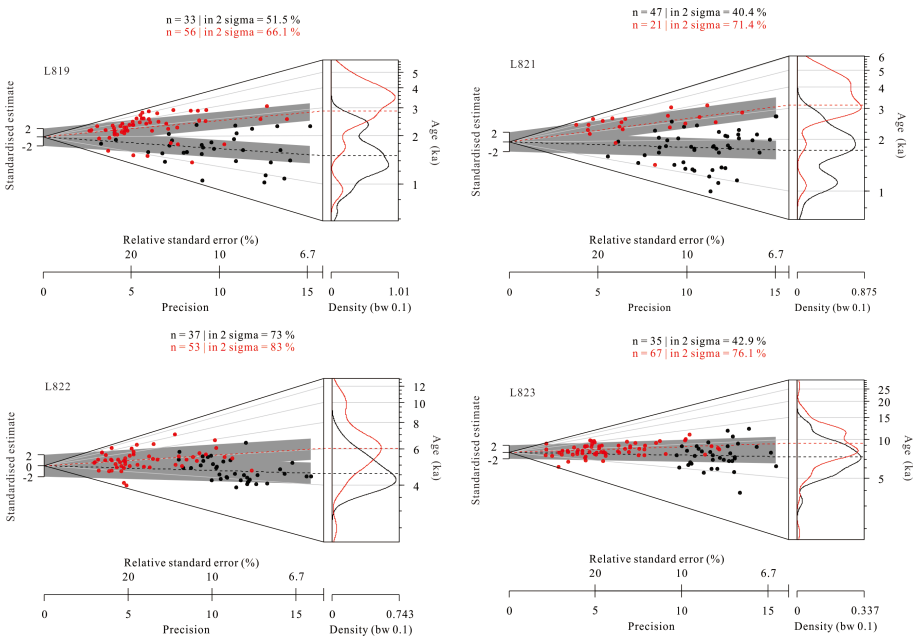

FIGURE 4
Abanico plots showing the distributions of 45–63 μm single-aliquot OSL ages (black circles) and corresponding 90–125 μm single-grain OSL ages (red circles) for representative samples from core LDC.

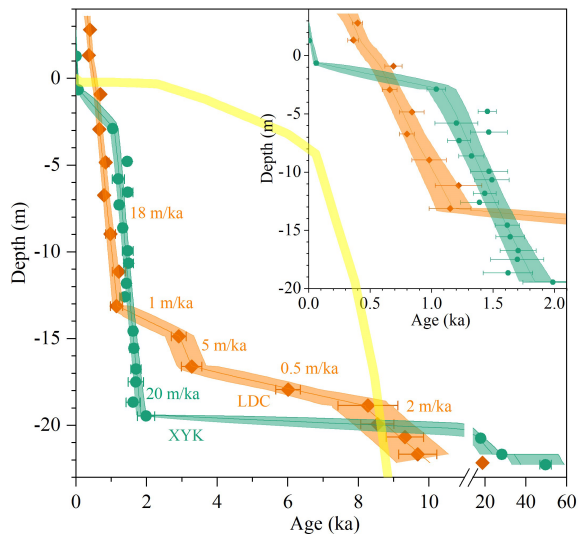

FIGURE 5
Age-depth models for core LDC (this study) and core XYK (Nian et al., 2022a), with the superimposed global sea-level curve (Lambeck et al., 2014). The models utilized sand-sized SG quartz OSL data for sandy layers (Supplementary Table S8) and silt-sized SA quartz OSL ages for silty layers (Supplementary Table S5). Orange diamonds represent the OSL ages from core LDC, while green circles correspond to those from core XYK. The solid lines depict the 'best-fit' age-depth relationships, with shaded areas indicating the 95% quantile range of the modelled age distributions. The inset details the age-depth model over the last 2 ka, showing alternating rapid deposition periods in the two cores.

Alternatively, this could be attributed to water turbidity and sediment source change. Prior to its southern migration in 1128 CE, the Yellow River discharged into Bohai Bay. Previous studies have revealed that limited Yellow River sediment would have entered the study area through longshore transport, with most sediment accumulating off the coast of the Shandong Peninsula (Yang and Liu, 2007; Hu et al., 2018). The long-term stability of the northern Jiangsu coastline before the Song Dynasty also suggests a deficiency of sediment supply (Zhang, 1984). Therefore, the coast is expected to have low water turbidity during that period. The sediments deposited above 11 m depth are dated from 0.4 to 0.9 ka, coinciding with the Yellow River's southward migration between 1128 and 1855 CE (Zhang, 1984). This migration likely introduced a shift in sediment provenance to the study area, with an increased influence from the Yellow River (Zhang et al., 1998). The Yellow River, famous for its huge sediment load over the last 1000 years (Wu et al., 2020), can lead to elevated water turbidity at the coring site, potentially affecting the bleaching conditions of the deposited sediments. Despite the anticipated impact of increased turbidity, the upper 11 m still shows better bleaching, suggesting that turbidity alone did not adversely affect the bleaching conditions of the sand-sized grains.

Previous studies have suggested that sediments in the study area are largely a mixture of the Yangtze and Yellow River sediments (Li et al., 2001). Therefore, differences in sediment provenance can account for such a difference. Since the southern migration of the Yellow River occurred in the last 0.9 ka, it is quite reasonable that the upper part of the core is characterized by a higher contribution of sediments from the Yellow River, while the deeper layers are predominantly influenced by the Yangtze River sediments. Considering sediments from the two large rivers show distinct geochemical and mineralogical compositions (Yang et al., 2002; Zhang et al., 2008, 2012), it is expected that they would exhibit differences in OSL characteristics. This interpretation is further supported by luminescence sensitivity variations observed in core HM from the Yangtze River Delta, where sediments older than 2 ka exhibit characteristics typical of the Yangtze, while younger sediments (0.4–0.6 ka) show a greater influence from the Yellow River (Nian et al., 2021).

These findings highlight the combined effects of incomplete bleaching, variations in turbidity, water depth, and shifts in sediment provenance that influence the temporal variations in luminescence signals of the tidal sandy ridges. Further studies can explore the sediment provenance tracing ability of OSL signals in the area.

4.3 Environment evolution history during the Holocene

The paleosol at the bottom of the stratigraphy has been dated to ~18.7 ka, and the hiatus between the paleosol and the overlying Holocene sediments suggests that the area remained subaerial for thousands of years due to lower sea levels from the Last Glacial Maximum through the early Holocene (Lambeck et al., 2014). Between 10–8 ka, the study area was influenced by rapidly rising sea levels characteristic of the early Holocene, which facilitated the formation of an initial tidal flat followed by estuarine facies. During this period, sedimentation rates were relatively high (Figure 5), comparable to those observed in the paleo-incised valley of the Yangtze River Delta to the south of the BTSB region (e.g., Nian et al., 2018a, 2018b, 2021). From 8 to 1.2 ka, deposition rates slowed, with a brief increase around 3 ka (Figure 5), indicating a prolonged period of limited sediment input. This slowdown is also observed in the Yangtze delta during the middle Holocene, likely due to decreased sediment discharge to the delta and adjacent coastal regions (Hori and Saito, 2007; Wang et al., 2018). A marked increase in sedimentation rates occurred between 1.2 to 0.4 ka, reflecting the influence of southern migration of the Yellow River and its discharge into the Yellow Sea. Sediments from the Yellow River were transported southward as far as to the Yangtze River Delta (Zhang et al., 2008, 2012; Wang et al., 2020; Shang et al., 2021), contributing to the rapid accretion observed since ~1 ka in the BTSB region.

Core XYK, located closer to the current coastline, also exhibits variable sedimentation rates during the Holocene but shows almost no deposition until ~2 ka (Nian et al., 2022a), contrasting with the continuous deposition observed in core LDC (Figure 5). Core XYK experienced rapid accretion between 2.0–1.2 ka with a significantly high rate of ~20 m/ka. This rapid deposition precedes that of core LDC over the past 2 ka, although the final emergence of land at the XYK site occurred after that of core LDC. In the east part of the

central BTSB, three ^{14}C results from core JC-1203 suggested a deposition period for the tidal sand ridge between 3 and 5 ka (Xiao, 2015). Additionally, the dating results of cores from the central part of BTSB reveal that the sand ridge was developed mainly since 1128 CE, implying sediment supply from the Yellow River was important (He et al., 2023). These variations indicate a complex spatiotemporal pattern of coastal deposition. This highlights that the underwater topography does not consistently present a seaward-sloping profile, implying that land formation in the BTSB is not a gradual progradation from inland to the coast but rather a complicated process influenced by frequent sand ridge migration. This complexity underscores the necessity for more core sampling to fully understand land formation processes in the BTSB region.

5 Conclusions

This study provides a refined chronological framework for the southern part of the BTSB region through OSL dating of both silt-sized and sand-sized quartz. Our results show that below the 11 m depth in core LDC, sand-sized quartz OSL ages (90–125 μm) are consistently older than silt-sized OSL ages (45–63 μm), suggesting that sand-sized grains provide more reliable age estimates as demonstrated previously in the adjacent core XYK.

The difference between sand-sized SG-CAM and SG-MAM ages is smaller in the upper part (above ~11 m depth) compared to the lower part of core LDC. The top ~11 m of sediments are deposited over the last 0.9 ka, which correspond well with the southern migration of the Yellow River and its sediment discharge into the Yellow Sea during 1128–1855 CE. These OSL characteristics may be useful for differentiating between sediments from the Yellow River and the Yangtze River, which warrants further investigation.

The OSL ages reveal marked temporal variation in sedimentation rate. Core LDC, located at the western BTSB experienced rapid deposition during 0.4–1.2 ka and 8–10 ka, with slower rates in between, whereas the eastern core XYK shows a more recent deposition history primarily within the last 2 ka. This suggests that although eventual land emergence occurred earlier at the inland site, but the spatiotemporal variation of underwater topography is more complicated, and therefore detailed core sampling and dating are required to reveal the evolutionary history of the coastal plain.

Data availability statement

The original contributions presented in the study are included in the article/Supplementary Material, further inquiries can be directed to the corresponding author/s.

Author contributions

XN: Conceptualization, Formal analysis, Funding acquisition, Investigation, Methodology, Project administration, Resources, Supervision, Validation, Writing – original draft, Writing – review & editing. WZ: Conceptualization, Formal analysis, Funding acquisition, Investigation, Methodology, Resources, Validation, Writing – original draft, Writing – review & editing. XW: Formal analysis, Investigation, Methodology, Validation, Writing – original draft, Writing – review & editing. FQ: Data curation, Formal analysis, Investigation, Methodology, Writing – original draft, Writing – review & editing.

Funding

The author(s) declare financial support was received for the research, authorship, and/or publication of this article. We gratefully acknowledge the National Natural Science Foundation of China for the financial support for this research (Grant Nos. 42171009 and 41771009).

Acknowledgments

We would like to express our sincere gratitude to Professors Li Wu and Zhongbo Wang for their constructive comments.

Conflict of interest

The authors declare that the research was conducted in the absence of any commercial or financial relationships that could be construed as a potential conflict of interest.

Publisher's note

Supplementary material

The Supplementary Material for this article can be found online at: https://www.frontiersin.org/articles/10.3389/fmars.2024.1500949/full#supplementary-material

References

Arnold, L. J., Bailey, R. M., and Tucker, G. E. (2007). Statistical treatment of fluvial dose distributions from southern Colorado arroyo deposits. *Quat. Geochronol.* 2, 162–167. doi: 10.1016/j.quageo.2006.05.003

Bailey, R. M., and Arnold, L. J. (2006). Statistical modelling of single grain quartz D_e distributions and an assessment of procedures for estimating burial dose. *Quat. Sci. Rev.* 25, 2475–2502. doi: 10.1016/j.quascirev.2005.09.012

Ballarini, M., Wallinga, J., Wintle, A. G., and Bos, A. J. J. (2007). A modified SAR protocol for optical dating of individual grains from young quartz samples. *Radiat. Meas.* 42, 360–369. doi: 10.1016/j.radmeas.2006.12.016

Burow, C. (2020). "calc_AliquotSize( ): Estimate the amount of grains on an aliquot. Function version 0.31, 2020," in *Luminescence: Comprehensive Luminescence Dating Data Analysis. R package version 0.9.7*. Eds. S. Kreutzer, C. Burow, M. Dietze, M. C. Fuchs, C. Schmidt, M. Fischer and J Friedrich. Available at: https://CRAN.R-project.org/package=Luminescence.

Chen, B., Li, C., and Ye, Z. (1994). The study on holocene sedimentation in the Southern South Hnanghai Sea coastal land. *Acta Sedimentologica Sin.* 12, 63–71.

Cheng, Q., Wang, F., Chen, J., Ge, C., Chen, Y., Zhao, X., et al. (2020). Combined chronological and mineral magnetic approaches to reveal age variations and stratigraphic heterogeneity in the Yangtze River subaqueous delta. *Geomorphology* 359, 107163. doi: 10.1016/j.geomorph.2020.107163

Cunningham, A. C., and Wallinga, J. (2010). Selection of integration time intervals for quartz OSL decay curves. *Quat. Geochronol.* 5, 657–666. doi: 10.1016/j.quageo.2010.08.004

Dyer, K. R., and Huntley, D. (1999). The origin, classification and modelling of sand banks and ridges. *Cont. Shelf Res.* 19, 1285–1330. doi: 10.1016/S0278-4343(99)00028-X

Galbraith, R. F., Roberts, R. G., Laslett, G. M., Yoshida, H., and Olley, J. M. (1999). Optical dating of single and multiple grains of quartz from Jinmium rock shelter, northern Australia: Part I, experimental design and statistical models*. *Archaeometry* 41, 339–364. doi: 10.1111/j.1475-4754.1999.tb00987.x

Gao, L., Long, H., Hou, Y., and Feng, Y. (2022). Chronology constraints on the complex sedimentary stratigraphy of the paleo-Yangtze incised valley in China. *Quat. Sci. Rev.* 287, 107573. doi: 10.1016/j.quascirev.2022.107573

He, L., Ye, S., Xue, C., Zhao, G., Yang, S., and Amorosi, A. (2023). Sedimentology and evolution of the Holocene radial tidal sand ridge in the south Yellow Sea, China. *Front. Earth Sci.* 10. doi: 10.3389/feart.2022.1107495

Hori, K., and Saito, Y. (2007). An early Holocene sea-level jump and delta initiation. *Geophys. Res. Lett.* 34, 18401. doi: 10.1029/2007GL031029

Hu, G., Xu, K., Clift, P. D., Zhang, Y., Li, Y., Qiu, J., et al. (2018). Textures, provenances and structures of sediment in the inner shelf south of Shandong Peninsula, western South Yellow Sea. *Estuar. Coast. Shelf Sci.* 212, 153–163. doi: 10.1016/j.ecss.2018.07.018

Jacobs, Z. (2008). Luminescence chronologies for coastal and marine sediments. *Boreas* 37, 508–535. doi: 10.1111/j.1502-3885.2008.00054.x

Lambeck, K., Rouby, H., Purcell, A., Sun, Y., and Sambridge, M. (2014). Sea level and global ice volumes from the Last Glacial Maximum to the Holocene. *Proc. Natl. Acad. Sci.* 111, 15296–15303. doi: 10.1073/pnas.1411762111

Li, C., Chen, Q., Zhang, J., Yang, S., and Fan, D. (2000). Stratigraphy and paleoenvironmental changes in the Yangtze Delta during the Late Quaternary. *J. Asian Earth Sci.* 18, 453–469. doi: 10.1016/S1367-9120(99)00078-4

Li, C., Zhang, J., Yang, S., and Fan, D. (1999). Characteristic and paleoenvironmental evolution of subaerial tidal sand body in Subei coastal plain. *Sci. China Ser. D: Earth Sci.* 42, 52–60. doi: 10.1007/BF02878498

Li, C. X., Zhang, J. Q., Fan, D. D., and Deng, B. (2001). Holocene regression and the tidal radial sand ridge system formation in the Jiangsu coastal zone, east China. *Mar. Geol.* 173, 97–120. doi: 10.1016/S0025-3227(00)00169-9

Li, C. X., and Zhao, J. (1995). Recent research and controversy of the Jianggang radial sand ridge in northern Jiangsu province. *Mar. Sci.* 4, 57–60.

Lin, P., Song, Y., Zhan, W., Tian, R., Wang, Z., Xu, X., et al. (2023). Late Pleistocene to Holocene sedimentary history in the Pearl River Delta revealed by OSL and radiocarbon dating. *CATENA* 224, 106972. doi: 10.1016/j.catena.2023.106972

Liu, J., Qiu, J., Saito, Y., Zhang, X., Nian, X., Wang, F., et al. (2020). Formation of the Yangtze Shoal in response to the post-glacial transgression of the paleo-Yangtze (Changjiang) estuary, China. *Mar. Geol.* 423, 106080. doi: 10.1016/j.margeo.2019.106080

Liu, R., Nian, X., Zhang, W., Qiu, F., Wang, Z., Lin, Q., et al. (2022). Luminescence dating of the late Quaternary sediments in Hangzhou Bay, China. *Quat. Geochronol.* 70, 101302. doi: 10.1016/j.quageo.2022.101302

Nian, X. M., and Zhang, W. G. (2018). Application of optically stimulated luminescence dating to Late Quaternary coastal deposits in China. *Quaternary Sci.* 38, 573–586. doi: 10.11928/j.issn.1001-7410.2018.03.03

Nian, X., Zhang, W., Liu, R., Qiu, F., and Seppä, H. (2024). Underestimated single-aliquot quartz OSL ages of Late-Pleistocene sediments due to the dominance of medium component. *Quat. Sci. Rev.* 332, 108656. doi: 10.1016/j.quascirev.2024.108656

Nian, X., Zhang, W., Qiu, F., and Liu, N. (2022a). The complexity of luminescence dating of tidal sand body revealed by the discrepancy of paired quartz OSL ages. *Quat. Geochronol.* 72, 101347. doi: 10.1016/j.quageo.2022.101347

Nian, X., Zhang, W., Qiu, F., Qin, J., Wang, Z., Sun, Q., et al. (2019). Luminescence characteristics of quartz from Holocene delta deposits of the Yangtze River and their provenance implications. *Quat. Geochronol.* 49, 131–137. doi: 10.1016/j.quageo.2018.04.010

Nian, X., Zhang, W., Wang, X., Hutchinson, S. M., Zhao, X., and Liu, K.-B. (2022b). Multi-centennial variability of yangtze delta growth over the last 2000 years: interplay of climate and people. *Earth's Future* 10, e2021EF002461. doi: 10.1029/2021EF002461

Nian, X., Zhang, W., Wang, Z., Sun, Q., and Chen, Z. (2021). Inter-comparison of optically stimulated luminescence (OSL) ages between different fractions of Holocene deposits from the Yangtze delta and its environmental implications. *Mar. Geol.* 432, 106401. doi: 10.1016/j.margeo.2020.106401

Nian, X., Zhang, W., Wang, Z., Sun, Q., Chen, J., and Chen, Z. (2018a). Optical dating of Holocene sediments from the Yangtze River (Changjiang) Delta, China. *Quat. Int.* 467, 251–263. doi: 10.1016/j.quaint.2018.01.011

Nian, X., Zhang, W., Wang, Z., Sun, Q., Chen, J., Chen, Z., et al. (2018b). The chronology of a sediment core from incised valley of the Yangtze River delta: Comparative OSL and AMS ^{14}C dating. *Mar. Geol.* 395, 320–330. doi: 10.1016/j.margeo.2017.11.008

Niu, W., Nian, X., Zhao, L., Zhai, Y., Meadows, M. E., Zhang, W., et al. (2022). Luminescence characteristics of muddy sediments in the turbidity maximum zone of the Yangtze River mouth and implications for the depositional mechanisms. *Front. Earth Sci.* 10. doi: 10.3389/feart.2022.972642

Shang, Y., Nian, X., Zhang, W., and Wang, F. (2021). Yellow River's contribution to the building of Yangtze Delta during the last 500 years-Evidence from detrital zircon U-Pb geochronology. *Geophys. Res. Lett.* 48, e2020GL091896. doi: 10.1029/2020GL091896

Wallinga, J. (2002). Optically stimulated luminescence dating of fluvial deposits: a review. *Boreas* 31, 303–322. doi: 10.1111/j.1502-3885.2002.tb01076.x

Wang, Z. Y. (1982). Discussion on the characteristics and origin of the relict sand of western South Yellow Sea. *Mar. Geol. Res.* 2, 63–70.

Wang, Y. (2014). *Environment and Resource of the Radial Sand Ridge Field in the South Yellow Sea* (Beijing: China Ocean Press).

Wang, Z., Saito, Y., Zhan, Q., Nian, X., Pan, D., Wang, L., et al. (2018). Three-dimensional evolution of the Yangtze River mouth, China during the Holocene: impacts of sea level, climate and human activity. *Earth Sci. Rev.* 185, 938–955. doi: 10.1016/j.earscirev.2018.08.012

Wang, F., Zhang, W., Nian, X., Roberts, A. P., Zhao, X., Shang, Y., et al. (2020). Magnetic evidence for Yellow River sediment in the late Holocene deposit of the Yangtze River Delta, China. *Mar. Geol.* 427, 106274. doi: 10.1016/j.margeo.2020.106274

Wintle, A. G., and Murray, A. S. (2006). A review of quartz optically stimulated luminescence characteristics and their relevance in single-aliquot regeneration dating protocols. *Radiat. Meas.* 41, 369–391. doi: 10.1016/j.radmeas.2005.11.001

Wu, X., Wang, H., Bi, N., Saito, Y., Xu, J., Zhang, Y., et al. (2020). Climate and human battle for dominance over the Yellow River's sediment discharge: From the Mid-Holocene to the Anthropocene. *Mar. Geology* 425, 106188. doi: 10.1016/j.margeo.2020.106188

Xiao, N. (2015). The sedimentary evolution research of coastal areas in Jianggang of Jiangsu province since Last Glacial Epoch. Ocean University of China, Qingdao, China.

Xu, X., Zhong, J., Huang, X., Li, H., Ding, Z., and Lai, Z. (2022). Age comparison by luminescence using quartz and feldspar on core HPQK01 from the Pearl River delta in China. *Quat. Geochronol.* 71, 101320. doi: 10.1016/j.quageo.2022.101320

Yang, C.-S. (1985). Discussion on genesis of Qianggang radial sand ridges. *Mar. Geology Quaternary Geology* 5, 35–44.

Yang, S. Y., Li, C. X., Jung, H. S., and Lee, H. J. (2002). Discrimination of geochemical compositions between the Changjiang and the Huanghe sediments and its application for the identification of sediment source in the Jiangsu coastal plain, China. *Mar. Geol.* 186, 229–241. doi: 10.1016/S0025-3227(02)00335-3

Yang, Z. S., and Liu, J. P. (2007). A unique Yellow River-derived distal subaqueous delta in the Yellow Sea. *Mar. Geol.* 240, 169–176. doi: 10.1016/j.margeo.2007.02.008

Zhang, R. S. (1984). Land-forming history of the Huanghe River delta and coastal plain of northern Jiangsu. *Acta Geographica Sin.* 39, 173–184. doi: 10.11821/xb198402005

Zhang, J., Li, C., and Cong, Y. (1998). Hydrodynamic environment and source of the old tidalsand body in the coastal plain of the northern Jiangsu. *Haiyang Xuebao* 20, 82–90.

Zhang, W., Ma, H., Ye, L., Dong, C., Yu, L., and Feng, H. (2012). Magnetic and geochemical evidence of Yellow and Yangtze River influence on tidal flat deposits in northern Jiangsu Plain, China. *Mar. Geol.* 319–322, 47–56. doi: 10.1016/j.margeo.2012.07.002

Zhang, W., Xing, Y., Yu, L., Feng, H., and Lu, M. (2008). Distinguishing sediments from the Yangtze and Yellow Rivers, China: a mineral magnetic approach. *Holocene* 18, 1139–1145. doi: 10.1177/0959683608095582